Josephson-Vortex-Flow Terahertz Emission in Layered High-T_c Superconducting Single Crystals

Myung-Ho Bae,[1] Hu-Jong Lee,[1,2] and Jae-Hyun Choi[1]

[1]*Department of Physics, Pohang University of Science and Technology, Pohang 790-784, Republic of Korea*
[2]*National Center for Nanomaterials Technology, Pohang 790-784, Republic of Korea*

(Received 11 September 2006; published 8 January 2007)

We report on the successful terahertz emission (0.6–1 THz) that is continuous and tunable in its frequency and power, by driving Josephson vortices in resonance with the collective standing Josephson plasma modes excited in stacked $Bi_2Sr_2CaCu_2O_{8+x}$ intrinsic Josephson junctions. Shapiro-step detection was employed to confirm the terahertz-wave emission. Our results provide a strong feasibility of developing long-sought solid-state terahertz-wave emission devices.

DOI: 10.1103/PhysRevLett.98.027002 PACS numbers: 74.72.Hs, 74.50.+r, 74.78.Fk, 85.25.Cp

Rapidly increasing applications of the electromagnetic (EM) waves in the terahertz frequency range (~0.1–30 THz) demand a novel technique of efficient terahertz-wave generation. Semiconductor EM-wave generating elements mainly rely on two operation principles: sinusoidal current oscillation and the transition of electronic states between quantum levels, which are realized by electronic and photonic means, respectively. However, terahertz-range EM-wave technology has remained underdeveloped (often dubbed the "terahertz gap") due to the following reasons: (i) in electronics, the transit of charge carriers in a semiconductor device inherently takes too long to produce the terahertz oscillation, while (ii) in photonics, the terahertz-range photon energy is much lower than the room-temperature ambient thermal energy. In spite of recent progress in assorted generation techniques [1–4] the terahertz generation remains to be a subject of intensive research efforts.

The present Letter describes the direct detection of the Josephson vortex-flow-induced terahertz-wave emission from $Bi_2Sr_2CaCu_2O_{8+x}$ (Bi-2212) stacked intrinsic Josephson junctions (IJJs). Since the size of the superconducting gap in Bi-2212 is higher than the Josephson plasma edge both the emission and the detection are allowed in a terahertz range [5]. In this study, the terahertz-wave emission was confirmed by observing Shapiro steps in an on-chip stack of IJJs (detector stack) as it was irradiated by the emission from the oscillator stack. The frequency of the emitted wave was tuned by the bias voltage, while the emission power was controlled by the bias current and switching of the resonating modes.

Naturally grown layered high-T_c superconducting Bi-2212 single crystals contain IJJs [6], where a 0.3-nm-thick superconducting CuO_2 bilayer and a 1.2-nm-thick insulating BiO-SrO layer alternate along the c axis. Since the superconducting electrodes in IJJs are much thinner than the c-axis London penetration depth λ_{ab} (~200 nm) the phase parameter ϕ_n in the nth Josephson junction is inductively coupled to those of neighboring junctions [7,8]. Thus, the electrodynamics, governed by coupled Sine-Gordon differential equations in a system of N stacked IJJs, is represented by the same number of standing Josephson plasma (SJP) collective eigenmodes formed along the c-axis direction. Josephson vortices generated by a planar external magnetic field tend to move in a tunneling bias current in resonance with the collective SJP modes, with the spatial phase distribution ranging from a rectangular (in-phase) to a triangular (out-of-phase) lattice. The maximum Josephson-vortex-induced emission can be achieved by tuning the vortex lattice to the in-phase rectangular SJP mode [9].

The conventional solid-state-reaction method was adopted to prepare Bi-2212 single crystals, which were slightly overdoped. The double-side-cleaving technique [10] was then employed to isolate and sandwich a finite number of Bi-2212 IJJs between two Au electrodes, essentially eliminating the interference from the pedestals (large stacks of IJJs outside of but coupled to the stack of IJJs of interest) and thus allowing the formation of ideal multiple SJP modes along the c-axis direction. We fabricated two specimens of stacked IJJs (SP1 and SP2). Fabrication details are described in Ref. [11]. Figures 1(a) and 1(b) show the schematic of the typical sample configuration and an scanning electron microscopy (SEM) image of SP2, respectively. The oscillator stacks were $13.5 \times 1.4\ \mu m^2$ [SP1] and $15.2 \times 1.9\ \mu m^2$ [SP2], while the detector stacks were $18 \times 1.3\ \mu m^2$ [SP1] and $11.6 \times 2.3\ \mu m^2$ [SP2] in their lateral dimensions.

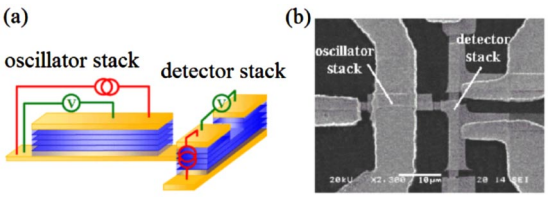

FIG. 1 (color online). (a) Schematic of sample and measurement configurations, showing the oscillator stack (left) and the detector stack (right) of intrinsic Josephson junctions. (b) SEM image of SP2.

The lower inset of Fig. 2 shows the oscillation of a Josephson-vortex-flow (JVF) resistance of SP1 ($N = 35$) as a function of external magnetic field at $T = 55$ K for a bias current of $I_b = 2$ μA. The field period of the oscillation, 0.51 kG, is one-half of H_0 [$= \Phi_0/Ld = 1.02kG$]. Here, H_0 is the magnetic field corresponding to a flux quantum Φ_0 through each junction of length L (=13.5 μm) and thickness d (=1.5 nm). The $H_0/2$ JVF resistance oscillation, known to originate from the interaction between a triangular vortex lattice and the edge potential for the vortex entry and exit at the junction boundaries [12,13], thus strongly indicates the formation of the triangular lattice in our oscillator stack in its low-bias static limit.

The upper inset of Fig. 2 exhibits a single JVF branch corresponding to the near-static triangular lattice in the low-bias region ($V < 23$ mV) and multiple quasiparticle branches in high biases at $T = 55$ K in a transverse field of $H = 1.2$ T; the field denoted by the arrow in the lower inset. In this field range, the single JVF branch persists down to $T = 4.2$ K (not shown). In a higher magnetic field of $H = 3.9$ T as in the region (ii) of the main panel of Fig. 2, however, the single JVF branch splits into multiple JVF sub-branches, which resulted from phase locking of a Josephson vortex lattice on multiple SJP modes [14,15]. SJP oscillations in each mode, standing along the c axis, propagate along junctions with a collective mode velocity [7,8], $c_n = c_0/\sqrt{1 - \cos[\pi n/(N+1)]}$. Here, n (=1–N) is the mode index and c_0 is the Swihart velocity, which governs the EM-wave propagation in a single Josephson junction.

In SP1 the JVF resistance oscillations are limited in the current bias range up to $I_b \sim 2$ μA. The multiple JVF sub-branches in the bias range of 2 μA $< I_b <$ 8 μA are clearly distinguished from the multiple quasiparticle branches above $I_b \sim 8$ μA, which corresponds to the critical current for the Josephson pair tunneling in the given magnetic field. In general, a stack of IJJs driven by a tunneling bias current in a planar magnetic field is in one of the three different dynamic Josephson-vortex states as illustrated in Figs. 2 and 3(a): (i) the near-static triangular vortex configuration, (ii) the multiple-mode dynamic vor-

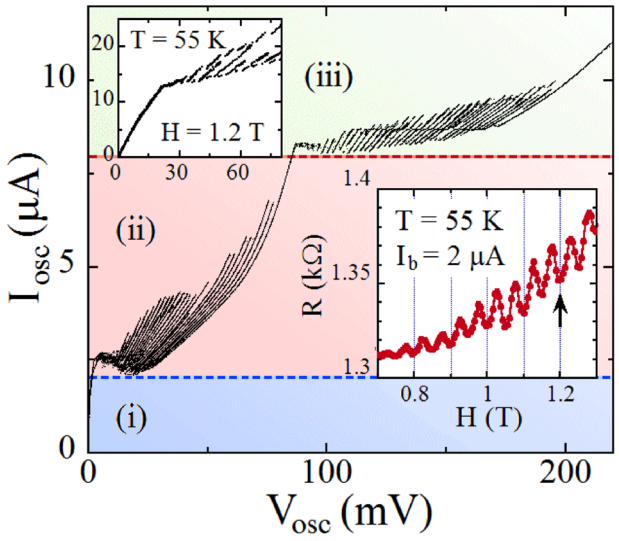

FIG. 2 (color online). I-V characteristics corresponding to the collective Josephson-vortex states (i), (ii), and (iii) refer to the main text of SP1 for $H = 3.9$ T at $T = 4.2$ K. The contact resistance was numerically subtracted. Upper inset: a single Josephson-vortex-flow (JVF) branch (low biases) and quasiparticle branches (high biases) in $H = 1.2$ T at $T = 55$ K, corresponding to the arrow position in the lower inset. Lower inset: JVF resistance versus external magnetic field of SP1 at $T =$ 55 K in a bias current of 2 μA.

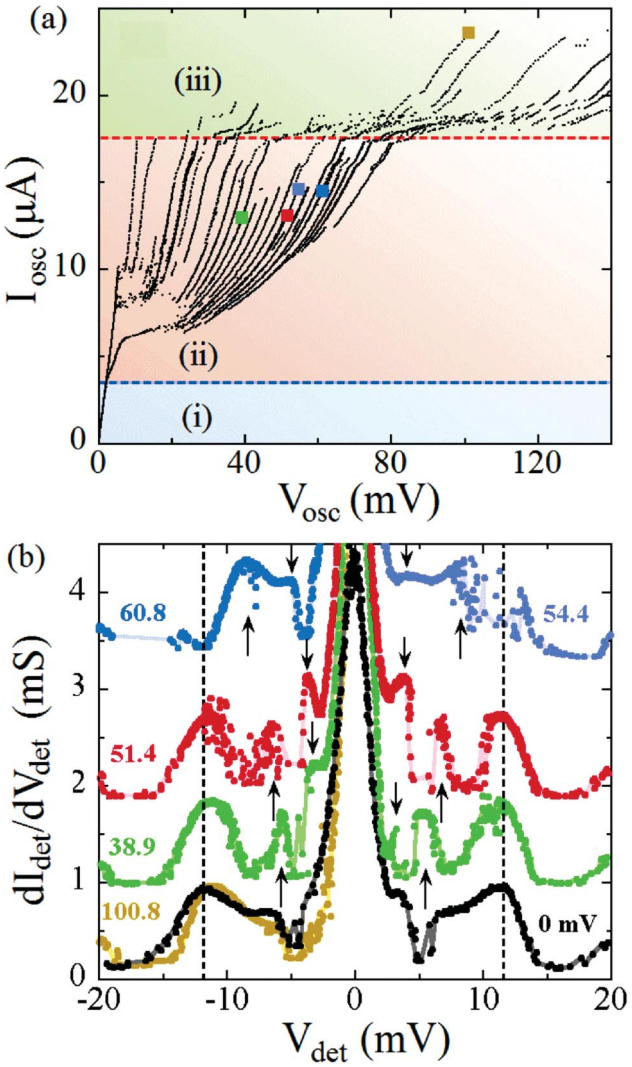

FIG. 3 (color). (a) Collective JVF multiple sub-branches and bias voltages V_{osc} (solid squares) of the oscillator stack of SP2 for $H = 4$ T at $T = 4.2$ K. The contact resistance was numerically subtracted. The states (i), (ii), and (iii) have the same characters as in Fig. 2. (b) Responses of the detector stack revealed in its differential conductance corresponding to the biases of the oscillator in (a). Each curve is shifted vertically for clarity.

tex configuration, and (iii) the irregular vortex configuration corresponding to the quasiparticle-tunneling state.

The maximum vortex-lattice velocity is governed by the propagation velocity of a resonating SJP mode. Thus, for the bias beyond $I_b \sim 8\ \mu$A, the JVF state transits to the quasiparticle tunneling state as the flowing vortices pass the state of the maximally allowed cutoff voltage $V_{\max}$, set by the highest plasma velocity in a junction. The maximum vortex-lattice velocity $c_{\max}$ in SP1 was estimated with $V_{\max}$ to be $\sim 3.8 \times 10^5$ m/s using the relation [15] of $V_{\max} = NHdc_{\max}$. The value of $c_{\max}$ should represent the fastest propagation mode among N collective SJP modes. The Swihart velocity estimated based on the resistively and capacitively shunted junction model [15,16] turns out to be $c_0 = 2.0 \times 10^4$ m/s. Then the corresponding highest in-phase mode velocity, $c_1 = 3.5 \times 10^5$ m/s, is in remarkable agreement with the observed value of $c_{\max}$ in SP1. This strongly implies that the last sub-branch [the rightmost branch in region (ii)] corresponds to the in-phase rectangular vortex lattice.

The moving vortex lattice that is in resonance with the collective transverse SJP oscillations is theoretically predicted to emit highly coherent EM waves at a junction edge [8,17]. The detection of the Shapiro steps, which arise as a result of the resonance between supercurrent oscillations and an irradiated microwave in a Josephson junction [18], would be the most direct confirmation of the EM emission from the sandwiched oscillator stack, with information on both the frequency and the power of the emission.

Figure 3(a) shows the bias conditions of the oscillator stack of SP2 ($N = 28$), $V_{\rm osc} = 38.9$, 51.4, 54.4, and 60.8 mV (denoted by solid squares in its JVF branches) and 100.8 mV (denoted in the quasiparticle branch), in a field of 4 T at $T = 4.2$ K. In SP2 the detector stack was coupled by the bottom Au electrode with the 2-μm interspacing to the oscillator stack.

The black $dI_{\rm det}/dV_{\rm det}$-vs-$V_{\rm det}$ curve at the bottom of Fig. 3(b) represents the response of the detector stack without any bias to the oscillator stack. The curve corresponds to simple nonlinear I-V characteristics without subbranches in the JVF region (not shown). The pronounced enhancement of the zero-bias conductance is due to Josephson-vortex pinning. The broad humps located in the vertical dotted lines are generated by the change in the slope of the detector I-V curves at the boundary ($V_{\max}$ of the detector) between the JVF and quasiparticle-tunneling regions. With much reduced detector-stack width facing the magnetic field (2.3 μm) not all the IJJs in the detector-stack took part in the vortex flow motion. The effective number of vortex-flowing junctions in the detector was estimated to be four by comparing values of $V_{\max}$ between the oscillator and detector stacks [19]. Here, we assumed the maximum velocity of the vortices was same in both stacks [20].

For a selected fixed bias to the oscillator stack in Fig. 3(a), two clear conductance peaks appear in the corresponding $dI_{\rm det}/dV_{\rm det}$-vs-$V_{\rm det}$ curve of the detector stack: $V_{\rm det}^{\rm prim}(V_{\rm det}^{\rm sub}) = 5.3 \pm 0.5\ (2.8 \pm 0)$, $6.6 \pm 0.2\ (3.7 \pm 0.2)$, $7.9 \pm 0.3\ (4.1 \pm 0.2)$, and $8.5 \pm 0.1\ (5.2 \pm 0.4)$ mV for four bias conditions in order of increasing voltages in the dynamic vortex state, respectively. Here, $V_{\rm det}^{\rm prim}$ and $V_{\rm det}^{\rm sub}$ are the voltage positions of the primary peak and the subpeak, which are denoted by the upward and the downward arrows, respectively, in Fig. 3(b). The voltage values of peaks in each curve shift in proportion to the increase of the bias voltage $V_{\rm osc}$ of the oscillator.

The voltages of the conductance peaks ($v_{\rm det}$) are plotted in Fig. 4(a) as a function of the bias voltage $v_{\rm osc}$. Here, $v_{\rm osc}$ ($\equiv V_{\rm osc}/N_{\rm osc}$) and $v_{\rm det}$ ($\equiv V_{\rm det}/N_{\rm det}$) are normalized by the number of junctions involved in the vortex flow in the oscillator and the detector stacks ($N_{\rm osc} = 28$ and $N_{\rm det} = 4$), respectively. For the primary peaks, the values of $v_{\rm osc}$ are in excellent accordance with the values of $v_{\rm det}$, which confirms that the primary peaks were caused by the Josephson ac response to the irradiation [21], i.e., integer Shapiro steps [22]. Frequencies corresponding to $V_{\rm osc} =$ 38.9, 51.4, 54.4, and 60.8 mV are 0.67, 0.87, 0.94, and 1.06 THz, respectively [23]. For the bias conditions of $V_{\rm osc} = 54.4$ and 60.8 mV, the humps at $V_{\max}$ in Fig. 3(b) smear out, as the outward-shifting positions of the conductance peaks overlap with those of $V_{\max}$.

In Fig. 3(b), $V_{\rm det}^{\rm sub}$ turns out to be one half of $V_{\rm det}^{\rm prim}$. The relation between the two kinds of peaks in terms of reduced parameters is shown in Fig. 4(a). These half-integer Shapiro steps are believed to be caused by phase locking of the second harmonics of the Josephson oscillations on the primary frequencies [24]. For the bias voltage of 100.8 mV in the quasiparticle-tunneling state of the oscillator stack, without the vortex-lattice formation along the c axis, no effective JVF-induced emission is expected. Thus, as in Fig. 3(b), the response of the detector without any Shapiro-step peaks in this bias is almost identical to the black zero-bias curve.

The irradiation power P is estimated from the approximate relation [25], $P \sim \Delta I_1^2 V_1 \Omega^2 \beta_c / 2 I_c$, where ΔI_1 is the height of the Shapiro current step, V_1 is the voltage value of

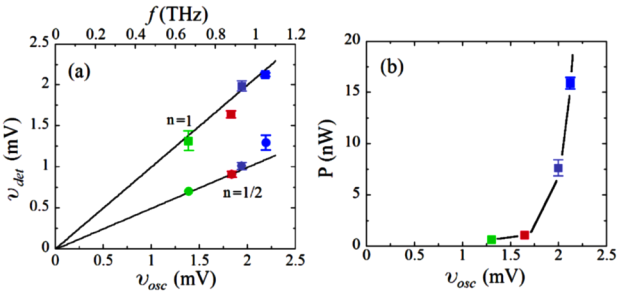

FIG. 4 (color online). (a) Primary ($n = 1$) and subharmonic ($n = 1/2$) conductance-peak voltages in the detector stack, corresponding to the integer and the half-integer Shapiro steps, respectively, with the emission frequencies denoted in the upper horizontal axis. (b) Estimated power irradiated on the detector stack for each bias condition in the oscillator stack.

the primary peak position, $\Omega^2\beta_c = (\pi h/e)(\epsilon f^2/tJ_c)$, $\Omega = f/f_c$ is the irradiated-wave frequency normalized by the characteristic frequency $f_c = 2eI_cR_n/h$, β_c is the McCumber parameter, ϵ is the dielectric constant, $t(=1.2$ nm) is the spacing between neighboring CuO_2 layers, and I_c (J_c) is the tunneling critical current (density). The value of ΔI_1 is estimated using the relation $\Delta I_1 = \Delta V_1 \frac{dI}{dV}|_{\text{prim}}$, where ΔV_1 is the voltage width of the primary peak [22] estimated at the base level of each curve in Fig. 3(b). Figure 4(b) illustrates that the estimated power irradiated onto the detector stack increases rapidly for lower-index modes; $P = 0.69 \pm 0.14$, 1.01 ± 0.16, 7.5 ± 0.7, and 15.9 ± 0.5 nW for the biases of $v_{\text{osc}} = 1.39$, 1.84, 1.94, and 2.17 meV, respectively. The emission power from the SJP modes is indeed theoretically predicted to grow for lower-index modes as the emitted waves become more phase-coherent and reaches a maximum for the completely in-phase mode corresponding to $n = 1$ [8]. One also notices that the two bias conditions $V_{\text{osc}} = 51.4$ and 54.4 mV in Fig. 3(a), even in the same branch, result in a large difference in the estimated irradiation power as in Fig. 4(b). This takes place because, as the vortex motion approaches the resonance condition in a branch, the energy fed by the bias is consumed more for an emission rather than speeding up the vortex lattice. An improved impedance matching between the oscillator and the detector stacks by combining proper antennas in the system is expected to generate clearer Shapiro steps with higher emission power. The emission power should vary as the square of the total number of coherently emitting IJJs in the oscillator element [27]. Thus, the power can be significantly enhanced by compactly placing separate oscillator stacks, each containing as many IJJs (practically $\sim$100), in parallel with each other on a common ground electrode within the wavelength of emitted THz waves.

The JVF terahertz generation in stacked Bi-2212 IJJs has the great advantage of continuous and frequency-tunable nature of the generated waves. The coherency of the terahertz emission from the rectangular vortex-lattice configuration is another advantage of JVF technique over, for instance, the radiation in a quasiparticle-tunneling region where the phase coherence is lacking between radiations from adjacent junctions. This study provides a noble scheme of developing solid-state terahertz emission sources [28,29] that will eventually help bridge the terahertz gap.

This work was supported by the National Research Laboratory program administrated by Korea Science and Engineering Foundation (KOSEF). This Letter was also supported by POSTECH Core Research Program.

[1] B. Ferguson and X. C. Zhang, Nat. Mater. **1**, 26 (2002).
[2] R. Köhler *et al.*, Nature (London) **417**, 156 (2002).
[3] G. L. Carr *et al.*, Nature (London) **420**, 153 (2002).
[4] K. Kawase *et al.*, Appl. Phys. Lett. **80**, 195 (2002); W. Shi and Y. J. Ding, Appl. Phys. Lett. **84**, 1635 (2004).
[5] E. J. Singley *et al.*, Phys. Rev. B **69**, 092512 (2004).
[6] R. Kleiner, F. Steinmeyer, G. Kunkel, and P. Muller, Phys. Rev. Lett. **68**, 2394 (1992).
[7] S. Sakai, P. Bodin, and N. F. Pederson, J. Appl. Phys. **73**, 2411 (1993); R. Kleiner, Phys. Rev. B **50**, 6919 (1994).
[8] M. Machida and M. Tachiki, Curr. Appl. Phys. **1**, 341 (2001).
[9] V. P. Koshelets and S. V. Shitove, Supercond. Sci. Technol. **13**, R53 (2000); G. Hechtfischer, R. Kleiner, A. V. Ustinov, and P. Muller, Phys. Rev. Lett. **79**, 1365 (1997); M.-H. Bae and H.-J. Lee, Appl. Phys. Lett. **88**, 142501 (2006).
[10] H. B. Wang, P. H. Wu, and T. Yamashita, Appl. Phys. Lett. **78**, 4010 (2001).
[11] M.-H. Bae *et al.*, Appl. Phys. Lett. **83**, 2187 (2003).
[12] S. Ooi, T. Mochiku, and K. Hirata, Phys. Rev. Lett. **89**, 247002 (2002); S. M. Kim *et al.*, Phys. Rev. B **72**, 140504(R) (2005).
[13] M. Machida, Phys. Rev. Lett. **90**, 037001 (2003); A. E. Koshelev, Phys. Rev. B **66**, 224514 (2002); Recently, M. Machida proposed [Phys. Rev. Lett. **96**, 097002 (2006)] that the edge potential also generates a rectangular lattice in a steady state for a sufficiently short junctions.
[14] J. U. Lee *et al.*, Appl. Phys. Lett. **71**, 1412 (1997).
[15] M.-H. Bae and H.-J. Lee, Phys. Rev. B **70**, 052506 (2004).
[16] A. Irie, Y. Hirai, and G. Oya, Appl. Phys. Lett. **72**, 2159 (1998).
[17] M. Tachiki, M. Iizuka, K. Minami, S. Tejima, and H. Nakamura, Phys. Rev. B **71**, 134515 (2005).
[18] Y. J. Doh, J. Kim, K. T. Kim, and H. J. Lee, Phys. Rev. B **61**, R3834 (2000); H. B. Wang, P. H. Wu, and T. Yamashita, Phys. Rev. Lett. **87**, 107002 (2001).
[19] H. B. Wang *et al.*, Appl. Phys. Lett. **88**, 063503 (2006).
[20] G. Carapella and G. Costabile, Appl. Phys. Lett. **71**, 3412 (1997); G. Hechtfischer *et al.*, Phys. Rev. B **55**, 14 638 (1997).
[21] A. V. Ustinov *et al.*, IEEE Trans. Appl. Supercond. **7**, 3601 (1997).
[22] Y. I. Latyshev, M. B. Gaifullin, T. Yamashita, M. Machida, and Y. Matsuda, Phys. Rev. Lett. **87**, 247007 (2001).
[23] The frequency is estimated based on the frequency-voltage (per junction) conversion relation, $f = 2eV_{\text{osc}}/Nh$ ($= 483.6$ GHz/mV $\times V_{\text{osc}}/N$).
[24] K. K. Likharev, *Dynamics of Josephson Junctions and Circuits* (Gordon and Breach, New York, 1986).
[25] For the power formula, we used $P = I_{\text{ac}}^2 R_{\text{in}}/2$, where I_{ac} is the ac current amplitude of irradiated waves, $R_{\text{in}}(=N/2\pi fC)$ is the input impedance and C is the capacitance of a junction [26]. Since the irradiated power is expected to be low enough in this study the height of the current step varies in linear proportion to the irradiation amplitude, resulting in $\Delta I_1 \approx I_{\text{ac}}/\beta_c\Omega^2$.
[26] S. Rother, Ph.D. thesis, Physikalisches Institut III, Universität Erlangen-Nürnberg, Germany, 1998.
[27] P. Barbara, A. B. Cawthorne, S. V. Shitov, and C. J. Lobb, Phys. Rev. Lett. **82**, 1963 (1999).
[28] I. E. Batov *et al.*, Appl. Phys. Lett. **88**, 262504 (2006).
[29] K. Kadowaki, Sci. Technol. Adv. Mater. **6**, 589 (2005); S. Savel'ev *et al.*, Nature Phys. **2**, 521 (2006).